11th World Congress on Computational Mechanics (WCCM XI)
5th European Conference on Computational Mechanics (ECCM V)
6th European Conference on Computational Fluid Dynamics (ECFD VI)
Koharu Furuta and Makoto Yamamoto (Eds)

NUMERICAL INVESTIGATION ON DROPLET TEMPERATURE OF ICE CRYSTAL ACCRETION

KOHARU FURUTA[*] AND MAKOTO YAMAMOTO[†]

[*]Graduate School of Mechanical Engineering, Tokyo University of Science
6-3-1 Niijuku, Katsushika-ku, Tokyo, Japan
e-mail: j4513645@ed.tus.ac.jp

[†]Department of Mechanical Engineering, Tokyo University of Science
6-3-1 Niijuku, Katsushika-ku, Tokyo, Japan
email: yamamoto@rs.kagu.tus.ac.jp

Key Words: *Multiphysics-CFD, Jet Engine Core Icing, Super-cooled Water Droplets.*

Abstract. *This paper discusses the ice accretion in high-temperature environment occurred by super-cooled water droplets. In mid-1990s, it was known that ice accretion occurs in the engine core such as the low pressure compressor and the first stage of the high pressure compressor, where the temperature is about 30 °C. The ice accretion in the engine core is called as "ice crystal accretion" because ice crystals are considered as the main cause of this high-temperature icing. Some scenarios are given for the ice crystal accretion, and one of which is caused by super-cooled water droplets. However, it is not clarified that ice crystal accretion can occur by only super-cooled water droplets. In the previous study, we developed the icing simulation code which can be applied to the environment where the temperature is above the freezing point. The icing code was applied to a flat plate as a computational target in the previous study. We use an actual compressor stator blade instead of a flat plate in this study. Then, we simulate the ice accretion in high-temperature environment with various initial temperatures of super-cooled water droplets. It is investigated whether ice crystal accretion occurs by only super-cooled water droplets or not. The obtained results indicate that ice crystal accretion can occur by only super-cooled water droplets.*

1 INTRODUCTION

Ice accretion is a phenomenon that super-cooled water droplets or ice crystals in the atmosphere impinge on a body and form an ice layer. When it occurs in a jet engine, the shape change of iced blades makes aerodynamic performance worse, and the ingestion of shedding ice flakes causes serious mechanical damages to the fan and the compressor components. Since there is the risk to lead to the serious accidents by ice accretion in a jet engine, the prediction of ice accretion is necessary in the design process. The experimental investigations have been carried out to estimate the ice accretion, but it is too difficult to set actual icing conditions and the experiments need high cost. Therefore, computational fluid dynamics (CFD) is useful to predict or estimate the ice accretion. In CFD, icing conditions can easily be

set as parameters and CFD need not high cost.

Engine components such as a splitter, a nose cone, fan blades and fan exit guide vanes have been considered as the icing areas in a jet engine. However, in mid-1990s, it was known that the ice accretion occurs in the engine core such as the low pressure compressor and the first stage of the high pressure compressor, where the temperature is about 30 °C [1]. The ice accretion in the engine core is called as "ice crystal accretion" because there is a hypothesis that the ice crystal accretion mainly occurs when the engine ingests ice crystals. It causes the flame out of the engine since ice flakes shed from the compressor components flow into the combustor. Some scenarios are given for the ice crystal accretion, one of which is caused by super-cooled water droplets. However, the mechanism has not sufficiently been clarified yet. Moreover, the existing icing code is not available in the environment where the temperature is above the freezing point.

In our previous study, we developed a new icing code which is applicable to a warm environment by introducing the heat conduction computation inside a computational target [2]. We used a flat plate as a computational target for simplification. It came out that the wall temperature of the flat plate could fall to the freezing point by the interaction between the cooling effect by the super-cooled water droplets and the heat conduction in the flat plate. Then, it becomes clear that the ice accretion starts and grows where the wall temperature falls to the freezing point. In this study, our new icing code is applied to an actual compressor stator blade in stead of a flat plate. In addition, we take various initial temperatures of super-cooled water droplets and we investigate whether ice crystal accretion occurs by only super-cooled water droplets or not in case of the compressor stator blade.

2 COMPUTATIONAL APPROACH

Figure 1 shows the flow chart of the simulation algorithm in this study. First, a flow field around the compressor stator blade is computed. Then, properties of the super-cooled water droplet trajectory, such as the impingement points of droplets and the number of impingement droplets are estimated by a Lagrangian method. At last, the temperature of the stator blade and the icing mass are computed by the thermodynamics and the heat conduction computation. However, in this study, we ignore an influence of the icing shape on the flow field and the droplet trajectory, so re-mesh is not conducted. These computational approaches used in this study are described in detail below.

2.1 Flow field

It is supposed that the flow field is two-dimensional, compressible and turbulent. The governing equations are the Favre-averaged mass, the momentum and the energy conservation equations. Non-viscous terms and viscous terms in these equations are discretized by the Yee-Harten's second-order upwind TVD scheme [3] and the second-order central-difference scheme, respectively. Then, the time integration is carried out by the LU-ADI method [4] and turbulence is estimated by the standard k-ε model with Kato-Launder modification [5].

2.2 Droplet trajectory

Droplet trajectory computation based on a Lagrangian method is carried out to get

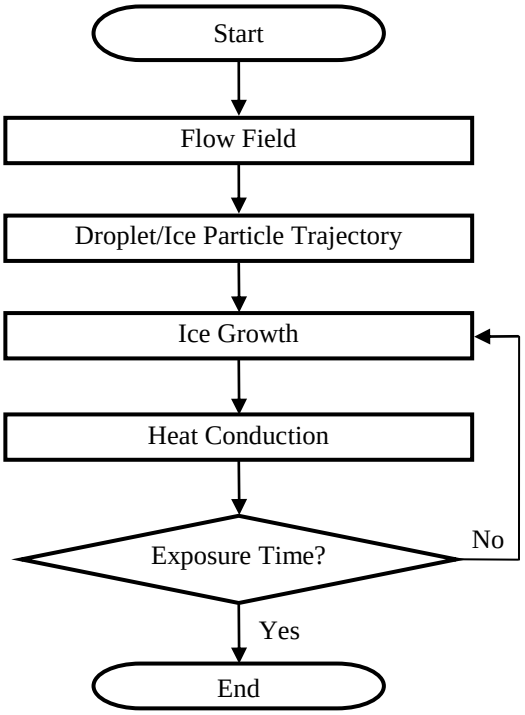

Figure 1: Algorithm of ice accretion simulation

properties of the droplet impingement on a wall surface. Since the drag is more than 80% in all forces acting on the droplet, only drag is taken into account and the other forces are ignored. Droplet-droplet collision, evaporation, merge and break-up are also ignored for simplification. It is supposed that the droplet is a complete sphere and does not make any effect on the flow field (One-Way Coupling). The simplified B-B-O (Basset-Boussinesq-Oseen) equation is used for the motion equation of a droplet. It can be computed by using the relative velocity between fluid and a droplet as described below,

$$\frac{d\vec{U}_w}{dt} = \frac{3}{4} C_D \frac{\rho_f}{\rho_w} \frac{1}{d_w} \vec{U}_r \left|\vec{U}_r\right| \tag{1}$$

where U_w is the water droplet velocity, U_r is the relative velocity of fluid and droplet, d_w is the water droplet diameter, ρ_f is the density of fluid, and ρ_w is the density of water droplet. C_D is the drag coefficient and obtained from the following formula in the Re_w range of 0.1 to 1000 (Schiller and Naumann, 1935). Re_w is the Reynolds number of a water droplet.

$$C_D = \frac{24}{\mathrm{Re}_w}\left(1 + 0.15\,\mathrm{Re}_w^{\,0.687}\right) \tag{2}$$

In addition, we set the hypothesis that flowing super-cooled water droplets do not change in state for simplicity.

2.3 Ice accretion

The Extended Messinger model [6] based on the Stefan problem is introduced for the ice

accretion computation in the present study. This model is governed by four equations; the heat conduction equations in ice and water layers, the mass balance equation in the ice and water layers, and the phase change condition at the ice/water interface,

$$\frac{\partial T_i}{\partial t} = \frac{k_i}{\rho_i C_{pi}} \frac{\partial^2 T_i}{\partial {y_w}^2} \tag{3}$$

$$\frac{\partial T_w}{\partial t} = \frac{k_w}{\rho_w C_{pw}} \frac{\partial^2 T_w}{\partial {y_w}^2} \tag{4}$$

$$\rho_i \frac{\partial B_i}{\partial t} + \rho_w \frac{\partial B_w}{\partial t} = m_{im} + m_{in} - m_{e,s} \tag{5}$$

$$\rho_i L_F \frac{\partial B_i}{\partial t} = k_i \frac{\partial T_i}{\partial y_w} - k_w \frac{\partial T_w}{\partial y_w} \tag{6}$$

where T_i and T_w are the temperatures, B_i and B_w are the thicknesses, k_i and k_w are the thermal conductivities, and C_{pi} and C_{pw} are the specific heats of ice and water, respectively. In Eq. (5), m_{im}, m_{in} and $m_{e,s}$ are impinging, runback and evaporating (or sublimating) water mass flow rates for a control volume, respectively. In Eq. (6), ρ_i is the density of ice, L_F is the latent heat by solidification and y_w is the distance from the wall. Equations (3)-(6) are integrated over time by the 4-step Runge-Kutta method. Each parameter used in the above equations is listed in Table 1.

2.4 Heat conduction

Heat conduction inside a wall is not considered in the existing icing simulation. The ice accretion has been considered as the phenomenon that super-cooled water droplets impinge on a body at low temperature environment, and the large temperature difference between a body surface and super-cooled water droplets does not arise. However, in case of high-temperature icing, the heat conduction is very influential because the temperature inside a wall changes from above the freezing point to the low temperature. In this study, the heat

Table 1: Parameter of extended Messinger model

Specific Heat of Ice	[J/kg K]	2,050
Specific Heat of Water	[J/kg K]	4,218
Thermal Conductivity of Ice	[W/m K]	2.18
Thermal Conductivity of Water	[W/m K]	0.571
Latent Heat of Solidification	[J/kg]	3.344×10^{5}
Density of Rime Ice	[kg/m^3]	880.0
Density of Glaze Ice	[kg/m^3]	917.0
Density of Water	[kg/m^3]	1,000
Heat Diffusivity	[m^2/s]	9.73×10^{-5}

conduction computation is introduced to the new icing code to simulate the high-temperature ice accretion. In order to estimate the temporal change of the temperature inside a wall, the heat conduction equation is employed,

$$\frac{\partial T_{in}}{\partial t} = a\left(\frac{\partial^2 T_{in}}{\partial x^2} + \frac{\partial^2 T_{in}}{\partial y^2}\right) \tag{7}$$

where T_{in} is the temperature in a stator blade, a is the thermal conductivity of a material, x and y are the parallel and vertical coordinates inside the wall, respectively. In Eq. (7), the coordinate system is different from that in the flow computation. The fine grid is used in the heat conduction computation because the scale of heat conduction is different from that of the flow field computation. The material of the stator blade used in this study is aluminum which has the high thermal conductivity.

3 COMPUTATIONAL CONDITIONS

3.1 Computational target and grid

In this study, we select the NACA65-210 airfoil as a compressor stator blade. The computational domain is shown in Fig. 2. The lengths from the leading edge to the inlet boundary and from the trailing edge to the outlet boundary are taken so as not to be influenced from the boundary condition. The length between the top and the bottom boundary is one pitch because of the geometrical periodicity.

The computational grid system has two sub grids based on the overset grid method to analyze in detail the flow field around the stator blade and the heat conduction inside the stator blade as indicated in Fig. 3. Note that the red grid is used only for the heat conductive simulation. The black grid is used for the computation of the flow field and the super-cooled water droplet trajectory. The blue grid is used to compute the properties of the super-cooled water droplet trajectory in detail. The total number of the grid points is about 300,000.

3.2 Computational condition

Computational conditions used in the ice accretion computation are summarized in Table 2. 1,000,000 droplets whose median volume diameter (MVD) is 20.0 μm are put in the inlet flow. Then, the collision mass of droplets on the wall is computed from the liquid water content (LWC). Here, LWC is determined to equal to the upper limit which is 8.0 g/m^3 (see

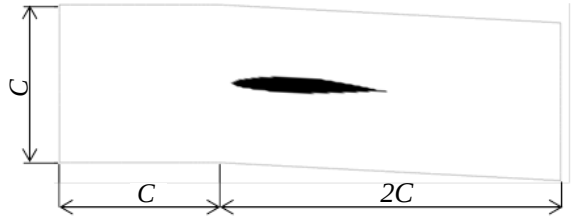

Figure 2: Computational domain and size

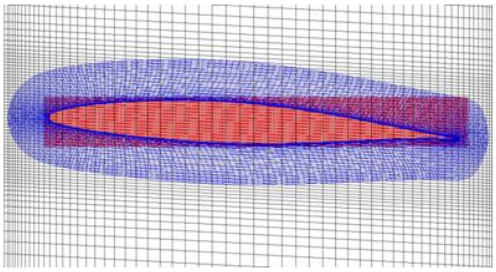

Figure 3: Computational grid system

Table 2: Computational condition

Chord Length	[m]	0.1
Angle of Attack	[deg.]	3.0
Inlet Velocity	[m/s]	244.3
Inlet Mach Number		0.7
Inlet Total Pressure	[MPa]	0.1497
Inlet Total Temperature	[K]	332.85
LWC (Liquid Water Content)	[g/m^3]	8.0
MVD (Median Volume Diameter)	[μm]	20.0
Inlet Droplet Temperature	[°C]	-30.0, -33.0, -37.0, -40.0
Exposure Time of Water Droplets	[s]	15.0

Ref. 1.) The thermodynamics computation for the super-cooled water droplets is performed till 15 sec. Inlet droplet temperature is set as -30, -33, -37 and -40 °C respectively.

3.3 Boundary condition

In the inlet boundary, the total temperature and the total pressure are fixed and the Mach number is extrapolated. In the outlet boundary, the static pressure is fixed and other variables are extrapolated. The periodic boundary condition is imposed on the top and the bottom boundaries. The wall is under no-slip, wall function and adiabatic conditions in the flow field computation. The temperature boundary condition at the wall surface in the heat conduction computation is computed by the Newton's law of cooling.

4 NUMERICAL RESULTS AND DISCUSSIONS

4.1 Flow field and local impingement number of super-cooled water droplets

Figure 4 shows the Mach number and the static temperature around the compressor stator blade. The stagnation point is generated at the leading edge and the static temperature increases to 324.3 K. Also, we can find the static temperature at the mid-chord of the suction side goes down to 267.7 K under the freezing point. From the Mach number in Fig. 4, it is obvious that the flow accelerates at the mid-chord of the suction and pressure sides. This is the reason why the temperature near the mid-chord decreases. This area can be likely to form an ice layer if this area catches super-cooled water droplets.

Figure 5 indicates the local impingement number of super-cooled water droplets when MVD is 20.0 μm and LWC is 8.0 g/m^3. The horizontal axis represents the stator blade position and the negative, zero and positive values denote the pressure side, the leading edge and the suction side of the stator blade, respectively. As indicated in Fig. 5, most droplets are collected near the leading edge and the pressure side (from the leading edge to the 40% chord position).

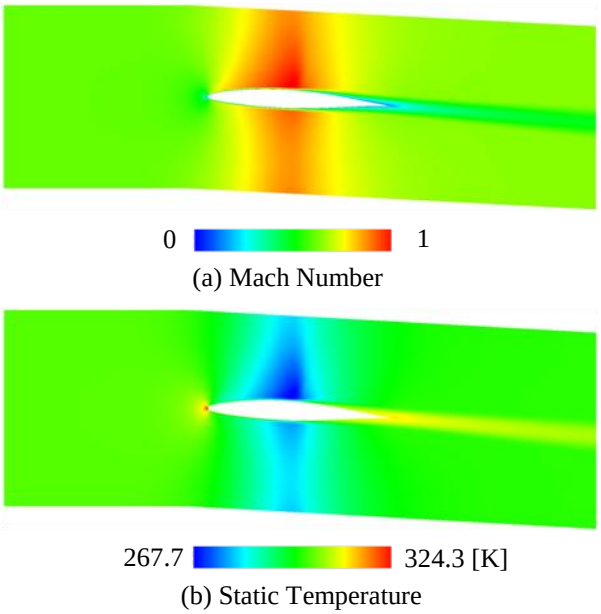

Figure 4: Mach number and static temperature

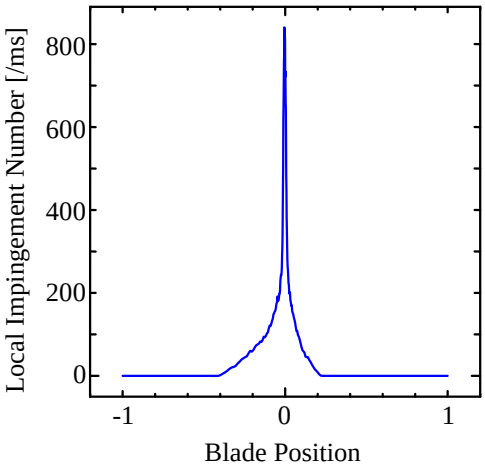

Figure 5: Local impingement number

4.2 Internal temperature of blade

Table 3 indicates the computational parameters of the ice accretion computation. Internal blade temperature distributions of each case are exhibited in Fig. 6. It is clear that the blade temperature decreases by the impingement of super-cooled water droplets. The cooling effect of super-cooled water droplets is large at the impingement point. Especially at the stagnation point, the blade surface temperature remarkably drops near the freezing point because the temperature difference between the stagnation point and impingement droplets is large.

On the other hand, the blade temperature near the mid-chord does not necessarily drop to the freezing point simply because the local static temperature is low. It is caused from that

Table 3: Computational parameter

Case	Inlet Droplet Temperature [°C]	Exposure Time [s]
1	-30.0	3.0
2	-30.0	15.0
3	-33.0	3.0
4	-33.0	15.0
5	-37.0	3.0
6	-37.0	15.0
7	-40.0	3.0
8	-40.0	15.0

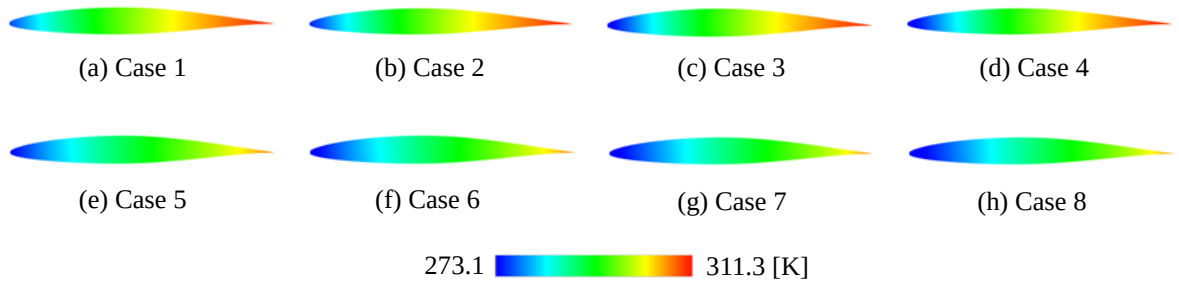

Figure 6: Internal blade temperature

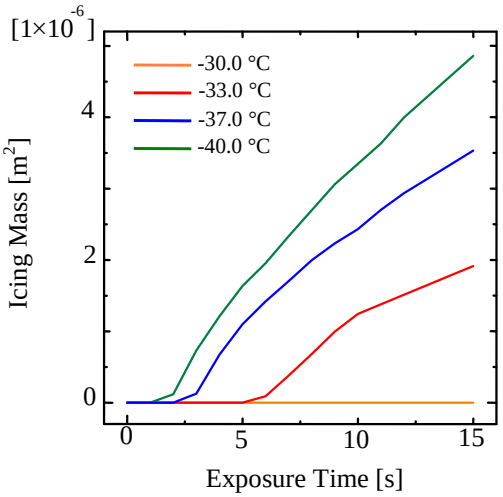

Figure 7: Temporal change of icing mass

droplets does not impinge on the mid-chord and the runback water into the mid-chord is heated by the surrounding warm air. In addition, the blade temperature around the leading edge decreases as the inlet droplet temperature comes down and the time has passed, because the cooling effect of droplets becomes large.

4.3 Icing mass

Temporal changes of the icing mass are shown in Fig. 7. It is obvious that the icing mass grows as the inlet droplet temperature decreases. Moreover, it is confirmed that the lower the droplet temperature is, the earlier icing starts. This is why a great deal of cooling effect is produced by the large temperature difference between the blade surface and impingement water droplets. Moreover, impingement water droplets likely to become the ice layer rather than the runback water when the droplet temperature is low.

In addition, it is found that the icing mass per unit time is larger when the temperature of super-cooled water droplets is lower. With low-temperature droplets, the warm runback mass flow rate decreases and the cooled surface area is expanded. That is why the ice growing rate increases in case of low-temperature water droplets.

5 CONCLUSIONS

We used the new icing code which is applicable to the environment where the temperature is above the freezing point. And it was applied to the compressor stator blade under super-cooled water droplet impingements. Obtained remarks in this study are summarized below.

- Ice crystal accretion can occur by only super-cooled water droplets in case of the present conditions.
- The internal blade temperature near the leading edge is remarkably cooled with the low temperature of super-cooled water droplets.
- The runback water warmed by the surrounding air makes the temperature of mid-chord difficult to decrease.
- The icing mass increases when the temperature of super-cooled water droplets decreases.

Our future prospects include that the temperature change of super-cooled water droplets should be conducted with the droplet trajectory computation. In addition, the temporal change of the droplet diameter will be computed.

REFERENCES

[1] G. Jeanne, J. Mason, Walter Strapp and Philip Chow, The Ice Particle Threat to Engines in Flight, *Proceeding of 44th AIAA Aerospace Sciences Meeting and Exhibit* (2006), 9-12.

[2] K. Furuta and M. Yamamoto, Numerical and Fundamental Study on Ice Growth of Ice Crystal Accretion, *Proceeding of APCOM & ISCM 2013* (2013), No. 1838.

[3] H. C. Yee, Upwind and symmetric Shock-Capturing Schemes. NASA-TM-89464 (1987).

[4] K. Fujii and S. Obayashi, Practical application of improved LU-ADI scheme for the three-dimensional Navier-Stokes computations of transonic viscous flows, *AIAA Paper* (1987), 86-0513.

[5] M. Kato and B. E. Launder, The modeling of turbulent flow around stationary and vibrating square cylinder, *Proceedings of 8th Symposium on Turbulent Shear Flows* (1993), 10-4-1-10-4-6.

[6] S. Ozgen and M. Canibek, Ice accretion simulation on multi-element airfoils using extended Messinger model, *Journal of Heat and Mass Transfer* (2009), Vol. 45, pp. 305-322.